J Heuristics (2007) 13: 227–242
DOI 10.1007/s10732-007-9017-3

Tomographic reconstruction using heuristic Monte Carlo methods

R. Barbuzza · M. Vénere · A. Clausse

Received: 16 May 2005 / Revised: 5 April 2006 / Accepted: 23 June 2006 / Published online: 30 March 2007

Abstract A tomographic reconstruction method based on Monte Carlo random searching guided by the information contained in the projections of radiographed objects is presented. In order to solve the optimization problem, a multiscale algorithm is proposed to reduce computation. The reconstruction is performed in a coarse-to-fine multigrid scale that initializes each resolution level with the reconstruction of the previous coarser level, which substantially improves the performance. The method was applied to a real case reconstructing the internal structure of a small metallic object with internal components, showing excellent results.

Keywords Tomography · Image reconstruction · Monte Carlo methods · Stochastic heuristics · Multigrid

1 Introduction

Computed tomography is a three-dimensional digital image of an object constructed from a certain number of projection measurements of the attenuated radiation passing through the object at different angles. The reconstruction of images from projections is important in a variety of problems including medical imaging diagnostics and non-destructive testing. Mathematically, the problem is to find the solution of the Radon anti-transformation of a spatial scalar field (Herman 1980). The conventional methods used to deal with this problem are the algebraic reconstruction, filtered back projection, and convolution back projection, along with many variants of these techniques (Herman 1980). While these methods perform quite well for reconstruction

R. Barbuzza · M. Vénere · A. Clausse (✉)
PLADEMA-ISISTAN, Universidad Nacional del Centro, 7000 Tandil, Argentina
e-mail: clausse@exa.unicen.edu.ar

M. Vénere · A. Clausse
CNEA-CONICET, 7000 Tandil, Argentina

problems with a complete set of projections having high signal-to-noise ratio, special cases benefit from alternative algorithms which can better model particular geometries and measurement processes. Examples of these cases appear in low dosage medical imaging (McKinnon and Bates 1981), non-destructive testing of materials with strong density variations (Sanderson 1979) and applications with limited angle projections (Inouye 1979) or hollow projections (Glover and Pelc 1981). In such cases, statistical methods can substantially improve the reconstruction quality by incorporating important prior information about either the imaging system or the imaged object.

Statistical heuristic methods resemble the random nature of physical processes, then seeking the solution that best matches the probabilistic behavior of the data. In cases of low signal-to-noise ratio, statistical methods can improve considerably the reconstruction performance. Statistical heuristics also deal easily with incomplete information such as limited or missing available data. Moreover, statistical techniques can incorporate implicit information about desired characteristics of the solutions.

The most frequently used statistical techniques for tomographic reconstruction are the Bayesian methods, which have been shown to improve performances in emission and transmission tomography problems (Geman and McClure 1985; Hebert and Leahy 1989; Green 1990; Sauer and Bouman 1993) and in image restoration (Hunt 1977; Geman and Geman 1984). Applications of the Metropolis Monte Carlo (MMC) method in image reconstruction for tomography and other physical problems can be found in the literature (Metropolis et al. 1953; Hammersley and Handscomb 1964; Chandler 1987; Gordon and Herman 1971; Frieden 1975; Kirkpatrick et al. 1983; Kearfott and Scott 1990; Matej et al. 1999; Chan et al. 1999; Winkler 2003). Matej et al. (1999) applied MMC to reconstruct a binary 2D image from projections and Chan et al. (1999) applied the method to recover gray images using Gibbs priors.

The present article presents a novel tomographic reconstruction approach based on MMC, which includes a heuristic procedure to guide the searching using the information contained in the projections. The novelty of the present technique is the use of adaptive heuristic samplings that assign higher probabilities to those regions of the image whose projections differ more from the projection data, thus increasing the convergence rate. Moreover, a multiscale algorithm is also included, which greatly reduce the computation time.

2 The Metropolis Monte Carlo method

MMC is a numerical method to approximate the solution of large optimization problems. Basically, in MMC the computer generates random samples in the domain containing the solution of a given mathematical problem, guided by a selection criterion that ensures the tendency toward the actual solution. This search produces a chronological sequence of configurations—called trajectory—for a particular system. This type of algorithms is ubiquitous in applied disciplines like engineering, molecular dynamics, computational biology, and many other fields.

For large non-trivial systems, the number of possible configurations is astronomically large, and therefore straightforward samplings of these configurations are im-

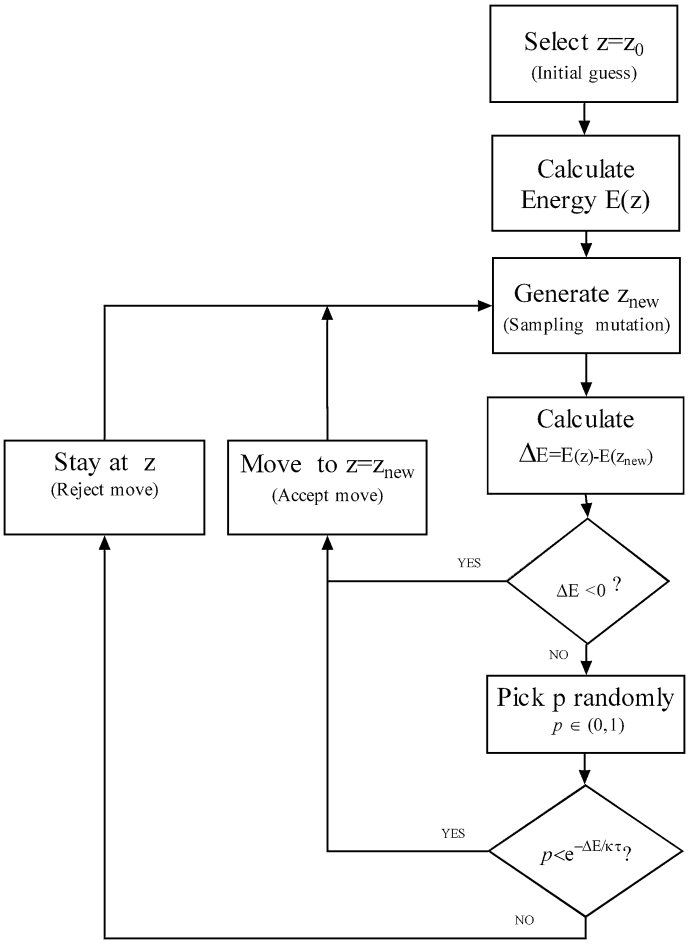

Fig. 1 Flowchart of the MMC algorithm for sampling in the canonical ensemble distribution

practical. In turn, MMC has a great deal of flexibility in choosing the particular random walk algorithm, bounding the search to a relatively small set of the total population representing some prior information that one might have from the optimal solution.

MMC is an optimization technique initially created to generate configurations of physical systems (atom lattices), with a probability proportional to $e^{-E/k\tau}$ where E is the energy associated to each configuration, τ is the temperature of the system, and k is the Boltzmann constant. After each execution of the random sequence the energy of the system changes by the amount ΔE. This energy difference ΔE governs the ratio of probabilities of the configurations, which is embedded into the MMC trajectory as a criterion for accepting or rejecting moves to new configurations. In other words, if the energy change is negative or null, the move is accepted. If the energy change is positive, the move is not rejected but it is accepted with probability $e^{-\Delta E/k\tau}$

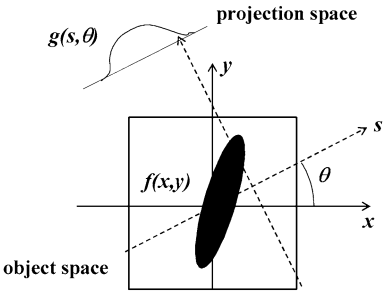

Fig. 2 Image space $f(x, y)$ and projection space $g(s, \theta)$

(Metropolis et al. 1953). The essence of the algorithm is described by the flowchart of Fig. 1. The variable z saves the current configuration of the system.

MMC is a particular case of the class of Markov-chains Monte Carlo methods (MCMC), which involves a Markov process generating a sequence of states $\{z^{(t)}\}$ whose probability depends on the previous state, $z^{(t-1)}$.

3 Monte Carlo in tomography reconstruction

Let us consider a planar cut of an attenuating body $f(x, y)$ as shown in Fig. 2. A set of parallel-beam, passing through the body at a given angle θ, produces a projection profile on a detector located opposite from the beam source. Thus, a projection at $\theta-$angle of $f(x, y)$, is a function defined over all ray s crossing the body, that is $g(s, \theta)$. For x-rays, $g(s, \theta)$ is defined as the logarithm of the ratio between the intensity $I(s, \theta)$ measured by the detector and the intensity of the x-ray source I_0. If the measured $I(s, \theta)$ is noiseless, the projection $g(s, \theta)$ is also referred as the Radon Transform of $f(x, y)$, that is:

$$g(s, \theta) = -\ln\left(\frac{I(s, \theta)}{I_0}\right) = \mathrm{R}f(x, y), \tag{1}$$

where $f(x, y)$ is the absorption coefficient of the object at the point (x, y), θ is the view angle, s is the line along which the beam travels in direction perpendicular to θ, and R is a matrix representing the Radon transformation. Each of the elements of R represents the cord length of the s-ray in direction θ across the pixel (x, y).

The image reconstruction involves estimating $f(x, y)$ from a set of its projections. That is, knowing M projections of a given object at different angles $\{\theta_1, \theta_2, \ldots, \theta_M\}$, the MMC tomographic reconstruction would perform a random search of the function $f(x, y)$ that satisfies (1), for every projected angle. In other words, the MMC algorithm will follow the steps shown in Fig. 1, where the z variable is $f(x, y)$ that will experience a series of random transformations.

In every step, the algorithm generates randomly a trial configuration $f^{(t)}$ within the set of all possible functions $f(x, y)$, guided by a selection criterion that ensures the convergence toward the actual attenuation field. The criterion for accepting the proposed changes is to minimize the square deviation of the projections produced by the sampled image, $f^{(t)}$, from the actual projections. The corresponding objective

function E is defined as:

$$E(f) = \sum_m \sum_n [g(s_n, \theta_m) - g_d(s_n, \theta_m)]^2, \tag{2}$$

where $g(s, \theta_m)$ and $g_d(s, \theta_m)$ are the projections at angle θ_m of a given trial f and the actual data projection respectively. In (2) the summation is performed over the N parallel rays $\{s_1, s_2, \ldots, s_N\}$ of each projection, for M different angles $\{\theta_1, \theta_2, \ldots, \theta_M\}$. $E(f)$ is treated as the "energy" of f (see Fig. 1), which will generate a statistical trajectory to minimize the deviation.

A similar procedure was implemented previously for binary images (i.e. black and white pixels) in hexagonal configuration (Matej et al. 1999). In that case the pixels to be changed are selected with uniform probability, which requires a huge number of iterations to converge. In the present study a different pixel selection criterion is introduced, which guides preferentially the random walk toward images that have relatively larger probability to be consistent with the actual data, increasing the speed of the reconstruction algorithm. Moreover, novel pixel-tone interchange rules and a multigrid convergence method are also included in order to enhance the algorithm efficiency.

The sequence of accepted images creates a Markov chain. The process of stabilization takes many iterations ending with images of similar energy, defined by (2). However, usually there are local minima that can also trap the trajectory. The problem of trapping in local minima is tackled using the Metropolis procedure (Metropolis et al. 1953); accordingly mutations increasing E are accepted with probability $e^{-\Delta E/k\tau}$, τ working as a tolerance (i.e., larger τ values tolerates larger increments of E), analogously to the temperature in statistical mechanics (Chandler 1987).

Some stopping condition must be specified in MMC algorithms. In this case the conditions are an imposed minimum E value or a maximum number of iterations. Until they both stabilized with images of similar energy.

Following the mentioned procedure, the MMC algorithm was implemented in C++ and applied to reconstruct planar figures from a finite set of projections. In the following sections, the *sampling* and *mutation* methods applied in the described algorithm are detailed.

3.1 Sampling methods

The pixel selection procedure in MMC is called sampling. The sampling of the pixel candidates for mutation trials is performed in the *Sample* method. Firstly, the selection is bounded to the set of pixels with finite intersection in all the projections (Fig. 3). Pixel-1 in Fig. 3 is a possible element in the selection process, for it belongs to a region where $g(s, \theta_1)$, $g(s, \theta_2)$ and $g(s, \theta_3)$ are greater than zero. In turn, pixel-2 is not selectable because $g(s, \theta_3)$ is null. This filter excludes those regions of the image from the selection mechanism, improving the efficiency of the algorithm.

There are two basic sampling methods in Monte Carlo (Hammersley and Handscomb 1964). The fixed sampling is a typical a priori plan established before the actual calculations. In the sequential sampling, the selection method depends on the observed numerical values found during the sampling. In our case, two sampling methods were designed.

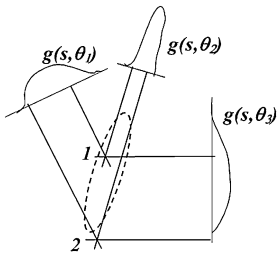

Fig. 3 Definition of the set of pixels: 1 is a valid pixel, 2 is not valid

3.1.1 Fixed sampling

In the fixed sampling, any possible pixel can be chosen from the set of candidate pixels with the same probability (i.e. uniform distribution). Firstly, a pixel is selected by intersecting two randomly chosen rays with different angle projection. To generate random rays a specified distribution $p(s, \theta_m)$ of the random variable S (set $\{s_1, s_2, \ldots, s_N\}$) is defined for each θ_m angle as:

$$p(s_j, \theta_m) = \begin{cases} 1/c_m & \text{if } g_d(s_j, \theta_m) > 0, \\ 0 & \text{elsewhere,} \end{cases} \tag{3}$$

where c_m is the quantity of parallel rays projected in direction θ_m satisfying that data projection $g_d(s_j, \theta_m) > 0$ ($j \in [1 \ldots N]$).

The *Fixed Sample* method is as follows:

1. Select randomly two projection angles θ_A and θ_B, where $A, B \in [1 \ldots M]$.
2. Sample two rays s_a and s_b ($a, b \in [1 \ldots N]$) guided by the probability density function $p(s, \theta_A)$ and $p(s, \theta_B)$ defined by (3).
3. Return the coordinates of the pixel (x_1, y_1), located in the intersection of s_a and s_b sampled rays.

3.1.2 Sequential sampling

In the sequential sampling the probability $p(s, \theta_m)$ of the random variable S (set $\{s_1, s_2, \ldots, s_N\}$) is recalculated in every step of the reconstruction, favoring those rays associated to the projections that differ more with the actual projection data, hence requiring larger correction.

Let $g(s, \theta_m)$ be the simulated projection of the current sample image at a given step. The square difference between $g(s, \theta_m)$ and the actual projection at angle θ_m and ray s, indicates the error of the corresponding ray. Hence, it is reasonable to expect that larger corrections are required in those pixels crossed by rays with high square difference. Following this line of reasoning, in each step, the candidate pixels can be selected by intersecting rays picked up with a probability:

$$p(s_j, \theta_m) = \frac{[g(s_j, \theta_m) - g_d(s_j, \theta_m)]^2}{\sum_n [g(s_n, \theta_m) - g_d(s_n, \theta_m)]^2}. \tag{4}$$

Accordingly *Sequential Sample* method proceeds as follows:

1. Select randomly two projection angles θ_A and θ_B, where $A, B \in [1 \ldots M]$.

2. Sample two rays s_a and s_b using the $p(s, \theta_A)$ and $p(s, \theta_B)$ distributions given by (4).
3. Return the coordinates of the selected pixel (x_1, y_1), located in the intersection of s_a and s_b sampled rays.

Apparently the sequential sampling requires higher computation than the fixed sampling, since (4) should be recalculated in every step of the reconstruction. However the acceptance rate is higher in the sequential sampling, and therefore it converges faster to the solution. On the other hand, the sequential sampling has a higher tendency to get trapped in local minima. The best heuristic alternative was to apply combinations of sequential and fixed samplings.

3.2 Mutation methods

An important aspect of MMC is the mutation amplitude applied to the sampled pixels. On one hand, if very small exchanges are applied in each mutation, the convergence would be very slow. On the other hand, too large mutation amplitudes would lead to noisy solutions. To manage this conflict, two strategies were implemented in the *Mutate* method: Assignment and Negotiation. In the Assignment, the tone of a sampled pixel is changed according to:

$$f_{\text{new}}(x, y) = f(x, y) + exchange,$$

where *change* is a value randomly generated within a certain uniform interval (f_{new} is the variable z_{new} in the flowchart of Fig. 1).

In the Negotiation, the mutation is the result of exchanging certain amount of tone between two sampled pixels (x_1, y_1) and (x_2, y_2), thus keeping constant the total intensity of the image. The corresponding mutation is given by:

$$f_{\text{new}}(x_1, y_1) = f(x_1, y_1) + exchange,$$
$$f_{\text{new}}(x_2, y_2) = f(x_2, y_2) - exchange.$$

The value *exchange* is initially large, and progressively is reduced as smaller corrections are required.

4 Monte Carlo multigrid

The multigrid method is based on the principle of recursive decomposition, similar to the divide-and-conquer methods (Aho and Ullman 1995). The underlying concept is to partition the domain of solutions in subdomains and combine them into a solution for the problem as a whole. In particular multigrid algorithms reconstruct the image at different resolutions, starting from a coarse resolution and progressing to the finest resolution. Frese et al. (1999), have applied the multiresolution framework in Bayesian reconstructions.

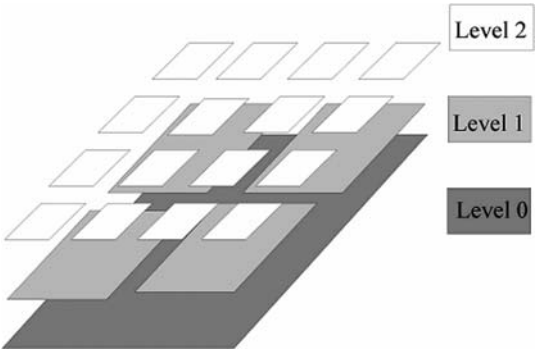

Fig. 4 Two-level reconstruction tree for Metropolis Monte Carlo Multigrid algorithm

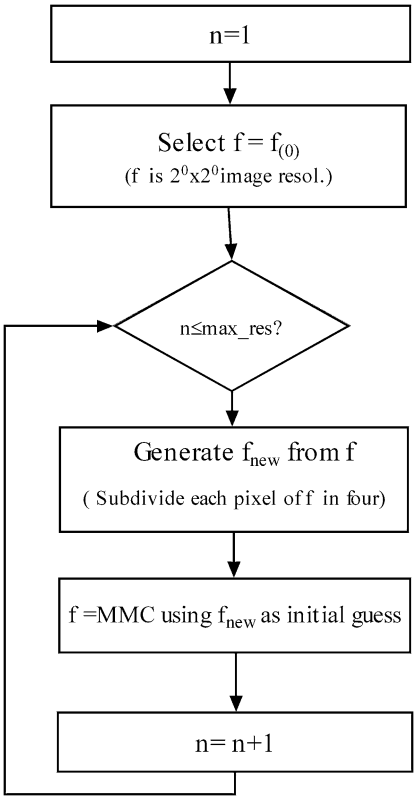

Fig. 5 Flowchart of the Multigrid MMC algorithm

5 Results

The performance of the MMC tomographic algorithm described above can be increased by implementing a multigrid procedure. For the n-level of resolution, the algorithm searches for an image of $2^n \times 2^n$ pixels by performing recursive decomposition into quadrants, progressively subdividing the grid until finally reaching the individual pixel (Fig. 4). The leaf nodes of the resulting tree represent the pixels. The nodes immediately above each leaf correspond to the $2^{n-1} \times 2^{n-1}$ image resolution.

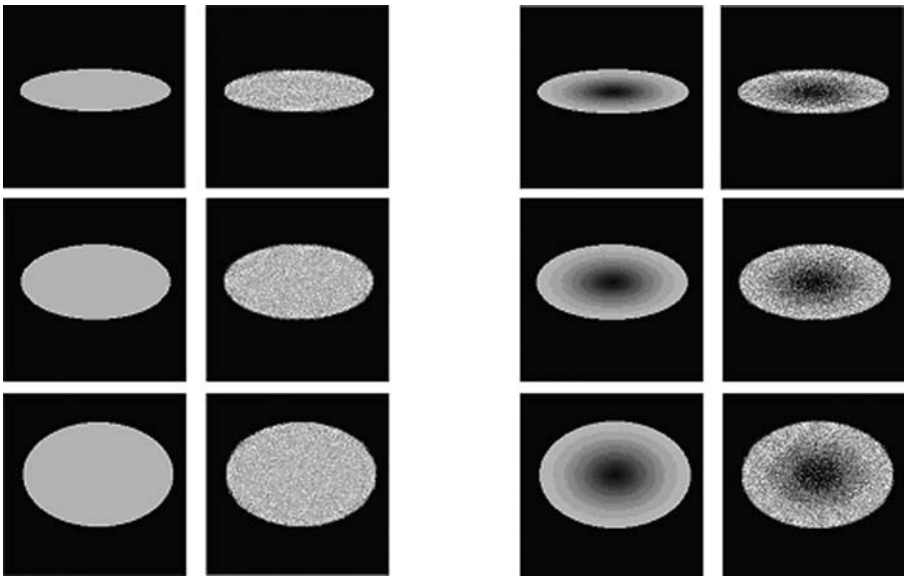

Fig. 6 MMC reconstructions of planar objects. Original ellipse phantoms of different eccentricity 0.3, 0.5 and 0.7, homogeneous (*left*) and non homogeneous (*right*). MMC reconstructed ellipses are shown beside the original ones

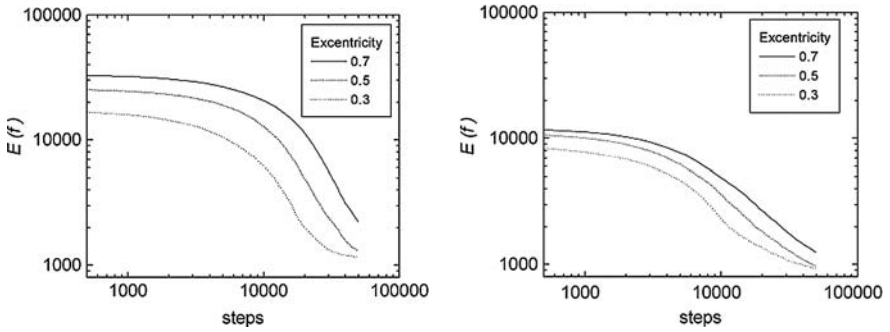

Fig. 7 Error evolution during MMC reconstructions of ellipses ($\tau = 0.5$). **a** Homogeneous filling, **b** gradient filling

The MMC algorithm is applied for each resolution level, taking the result of each level as the initial guess for the following finer level. Obviously, it is necessary to partition the reconstruction resulting in the $n - 1$ resolution in order to be consistent with the initial guess introduced in the n resolution level. Figure 5 describes the details of the multigrid procedure.

There are several significant advantages in using the multiresolution approach. While the plain MMC algorithm updates one pixel at a time, MMC-multigrid updates blocks of pixels per iteration in coarse levels, resulting in faster convergence.

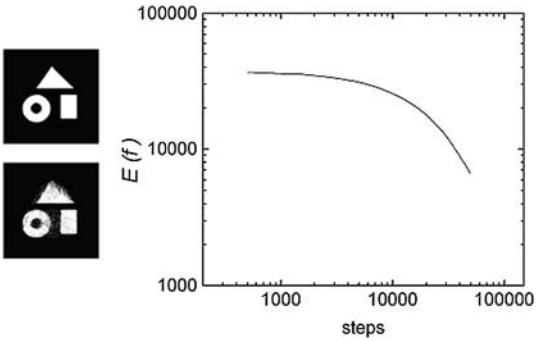

Fig. 8 Error evolution during MMC reconstructions of complex shapes

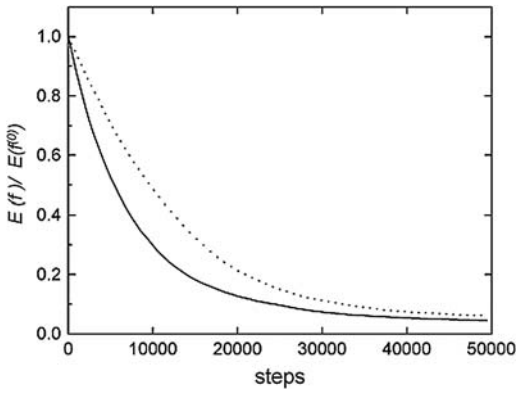

Fig. 9 Average error reduction during the reconstruction of the ellipses shown in Fig. 6, applying Negotiation mutation (*solid*) and Assignment mutation (*dashed*)

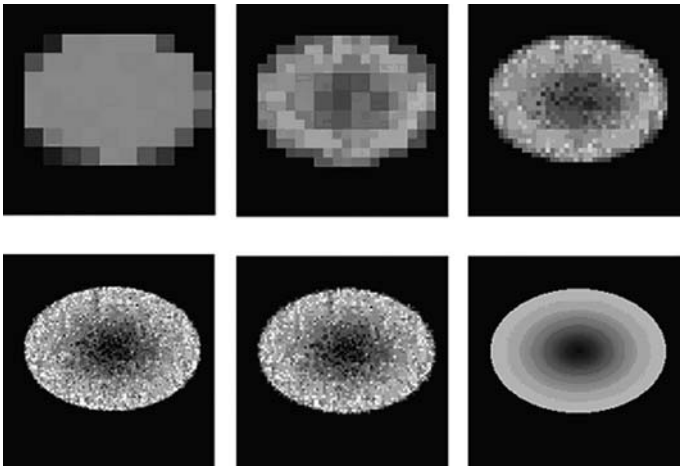

Fig. 10 Evolution of the Multigrid MMC reconstruction of an ellipse

This is due to the fact that the local interactions in coarse reconstructions are equivalent to large scale propagation at finer resolutions. Since the coarse reconstructions already contain the large scale behavior of the solution, substantially less iteration is necessary at the finer scales. Moreover, the coarse scale reconstructions are less com-

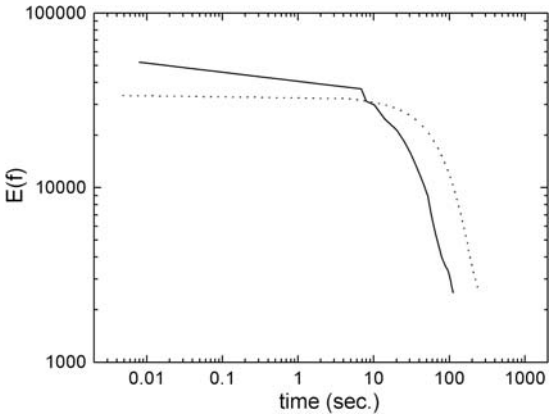

Fig. 11 Evolution of the image error (2) during MMC (*dashed*) and Multigrid MMC (*solid*) reconstructions of an ellipse

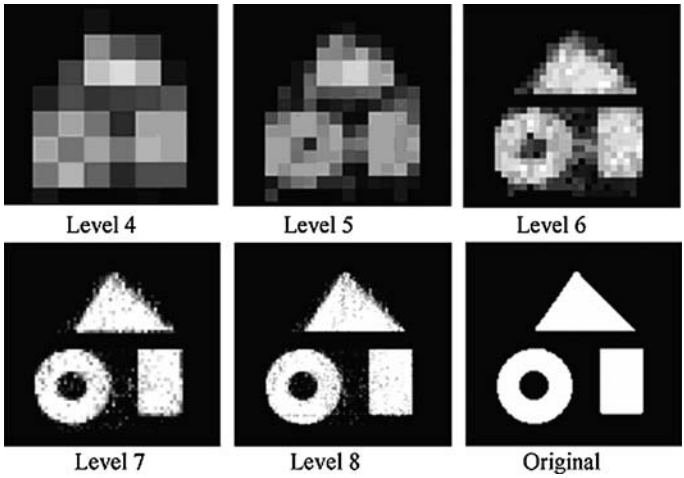

Fig. 12 Evolution of the Multigrid MMC reconstruction of a group of shapes

plex, and therefore require less iteration. In addition, the multiresolution algorithm is more robust with respect to local minima trappings during the optimization.

Figure 6 shows the performance of the MMC reconstruction on elliptical figures. Assignment mutations combined with sequential samplings were applied in the first 45000 steps, following by fixed samplings during the rest of the calculation. The reconstructions has been performed using eight projections corresponding to 0, 30, 60, 75, 90, 105, 120 and 150 degrees, 512 parallel beams each. Figure 7 shows the evolution of the error (2) between the true image and the reconstructed instances. It can be seen that the method succeeds in finding good reconstructions of simple shapes after a few tens of thousand steps. Figure 8 compares reconstructions with true images of more complex test phantoms. The trend of the error reduction is similar to Fig. 7.

Generally the mutation by Negotiation performs better than by Assignment. Figure 9 compares the average error reduction during the reconstruction of the ellipses shown in Fig. 6 applying Negotiation and Assignment mutations. It can be seen that

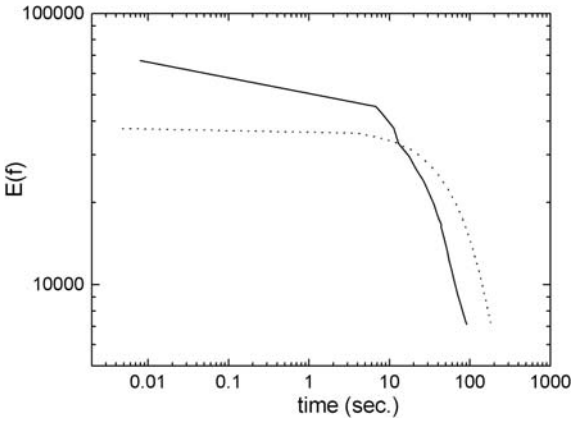

Fig. 13 Evolution of the image error (2) during MMC (*dashed*) and Multigrid MMC (*solid*) reconstructions of the group shown in Fig. 12

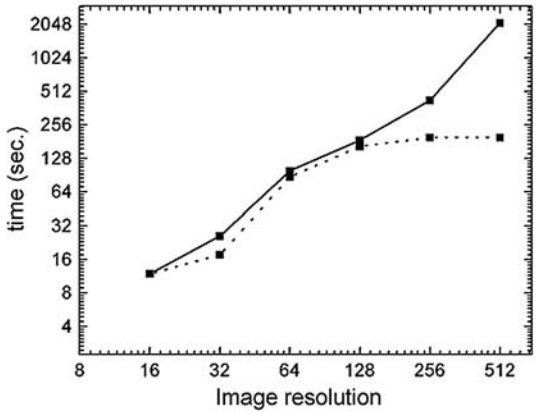

Fig. 14 Reconstruction of an ellipse using MMC (*solid*) and Multigrid MMC (*dashed*) with different coarsing levels

at the beginning of the reconstruction the error decreases sharply, although the reduction slows down later.

Figure 10 shows the evolution of an ellipse reconstruction during multigrid MMC ($2^8 \times 2^8$ image size). The progressive refining of the image can be appreciated at different coarsing levels. Figure 11 compares the error (2) evolution using plain and multigrid MMC. Initially the error of MMC-multigrid is higher because the solution is bounded to a coarse approximation of the image. However, at finer levels the error rapidly decreases. Using a AMD Athlon XP 1.8 GHz, after 10 seconds, both techniques reach the same error value. Afterwards, the multigrid reconstruction takes the lead.

Figure 12 shows the multigrid MMC reconstruction of a group of figures. Crude approximations of the image are achieved at the initial coarse levels. However, as the resolution level increases, better instances are obtained. The corresponding error evolutions are compared in Fig. 13. The multigrid algorithm scores considerable better in efficiency.

Reconstructions following multigrid generally converge faster than the plain MMC. However, the latter does not occur for images smaller than 256×256 pixels, since the computational cost of each multigrid mutation depends on the coarsing

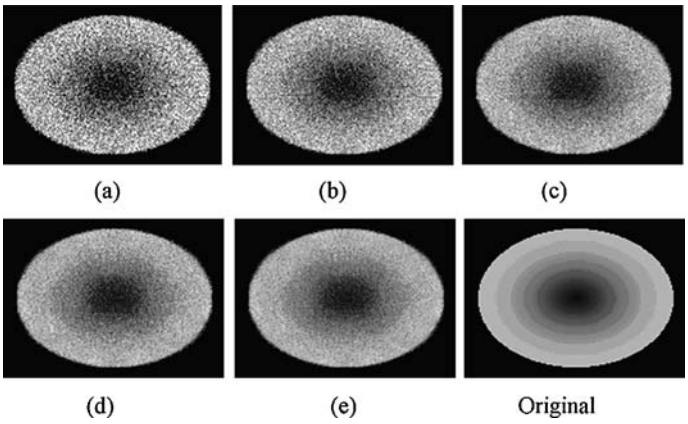

Fig. 15 Statistical refining of MMC reconstructions. The image obtained is an average of (**a**) two, (**b**) four, (**c**) six, (**d**) eight, and (**e**) ten reconstructions starting with different seeds

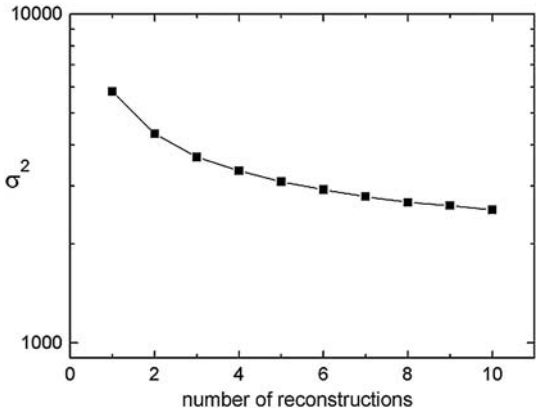

Fig. 16 Mean square error between the original ellipse and images averaging MMC reconstructions

level (i.e., mutations at finer levels are more expensive). In other words, the overhead cost of handling the tree of the multigrid data structure is not compensated if the image is small. The computational cost to reach multigrid convergence at the desired resolution level *maxres* is given by:

$$C(maxres) = \sum_{n=0}^{maxres} m_n c_n,$$

where m_n and c_n are the required number of mutations and the cost per mutation at the n-level of resolution. In plain MMC the reconstruction is performed only at resolution level *maxres*. For images with large number of pixels, the initial guess to the finest level substantially reduces the number of mutations required for convergence. For small images this effect is not sufficient to compensate the additional mutations required to converge in the coarser levels. Figure 14 shows the reconstruction times of the ellipse at of Fig. 8 at different coarsing levels (i.e. $2^n \times 2^n$, $n = 4, 5, 6, 7, 8$ and 9).

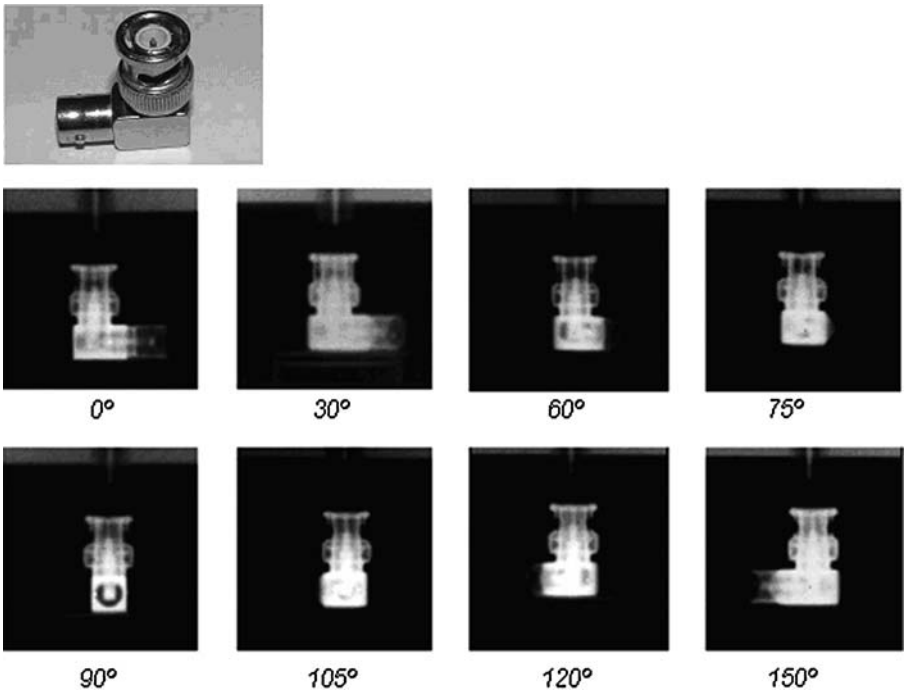

Fig. 17 Photograph of a BNC elbow and its 8 radiographs at different angles

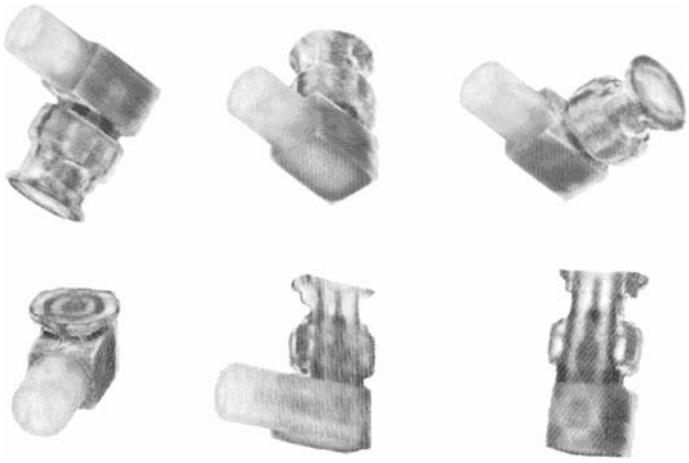

Fig. 18 3D visualization of the reconstructed BNC from 8 projections of Fig. 17 (*up*) and different cross section of the BNC (*bottom*)

For $maxres = 9$ multigrid are up to 20 times faster than plain MMC. The difference is considerably minor for smaller image sizes.

A typical drawback of MMC reconstructions is that the final images are often noisy representations of the original object. The reason of this undesirable feature

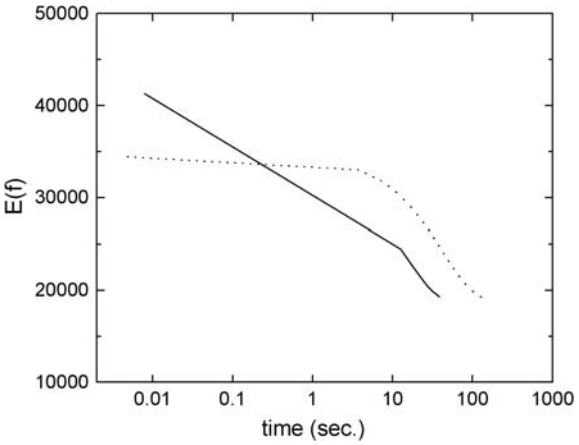

Fig. 19 Evolution of the error during the reconstruction of the BNC elbow using Multigrid MMC (*solid*) and plain MMC (*dashed*)

is that the errors of the projections of these noisy solutions differ only slightly from the corresponding projections of the original image, causing trappings of the searching trajectory in small local minima, which are practically impossible to overcome even using the Metropolis technique. A heuristic way to overcome this problem is by averaging a number of reconstructions using different pseudorandom number generation sequences, refining the final images by cancellation of positive and negative deviations. Figure 15 shows the reconstructions obtained with the statistical refining averaging different numbers of final images. Figure 16 shows how the mean square error compared with the original image is reduced as more reconstructions are added to the average.

An experimental radiographic session was performed using a pulsed x-ray source (Vénere et al. 2001). A stainless steel BNC elbow was mounted on a platform that rotates allowing projections at 8 different angles, namely 0, 30, 60, 75, 90, 105, 120 and 150 degrees. Data projections were limited in 512 beams. Figure 17 shows the set of radiographs of the piece at different angles. The length of the pixel side is 0.08 mm.

Reconstructions were performed using the plain and multigrid MMC algorithms. Figure 18 shows different views and cuts of the image reconstruction of the object. The resolution is about 0.3 mm. Figure 19 shows the evolution of the error (2) during the reconstruction of the BNC elbow using multigrid MMC (solid) and plain MMC (dashed). Multigrid MMC converges twice faster than plain MMC, and its final error is smaller. It can be seen that initially the multigrid MMC error is higher, since instances at coarse scales are limited approximations. However, multigrid MMC converges rapidly at lower levels of resolution.

6 Conclusion

The feasibility of good tomographic reconstructions by means of MMC methods was demonstrated. The introduction of MMC techniques in CT is promising among other things because they are suitable to include artificial intelligent strategies without changing the general structure of the reconstruction algorithm.

The behavior of fixed and sequential samplings was studied in test images, quantifying the efficiency gain of the latter. A mutation strategy which conserves the global image intensity was found appropriate and convenient for most reconstructions. In order to reduce the computational cost a multigrid scheme was implemented, which reduces the calculation time by 100% or more in standard size images. The final quality of the reconstructions can be enhanced by applying statistical averaging over several reconstructions.

The method was applied to a real case reconstructing the internal structure of a small metallic object with internal components, showing excellent results.

References

A. Aho, J. Ullman, Foundations of Computer Science (Computer Science Press, New York 1995)
T. Chan, G. Herman, E. Levitan, in Discrete Tomography: Foundation, Algorithms and Application, ed. by G.T. Herman, A. Kuba (Birkhäuser, Boston, 1999), pp. 214–233
D. Chandler, Introduction to Modern Statistical Mechanics (Oxford University Press, New York, 1987)
T. Frese, C.A. Bouman, K. Sauer, in Discrete Tomography: Foundation, Algorithms and Application, ed. by G.T. Herman, A. Kuba (Birkhäuser, Boston, 1999), pp. 237–264
B. Frieden, in Topics in Applied Physics, vol. 6 (Springer, Berlin, 1975), pp. 177–249
S. Geman, D. Geman, IEEE Trans. Pattern Anal. Mach. Intell. **6**, 721–741 (1984)
S. Geman, D. McClure, in *Proc. Stat. Comput. Sect. Am. Stat. Assoc.* (Washington, DC, 1985), pp. 12–18
G. Glover, N. Pelc, Med. Phys. **8**, 799–807 (1981)
R. Gordon, G. Herman, Commun. ACM **14**(12), 759–764 (1971)
P. Green, IEEE Trans. Med. Imaging **9**, 84–93 (1990)
J. Hammersley, D. Handscomb, Monte Carlo Methods (Chapman and Hall, New York, 1964)
T. Hebert, R. Leahy, IEEE Trans. Med. Imaging **8**, 194–202 (1989)
G.T. Herman, Image Reconstruction from Projection (Wiley, New York, 1980)
B. Hunt, IEEE Trans. Comput. **C-26**, 219–229 (1977)
T. Inouye, IEEE Trans. Nucl. Sci. **NS-26**, 2666–2684 (1979)
K. Kearfott, E. Scott, IEEE Trans. Med. Imaging **9**(2), 128–143 (1990)
S. Kirkpatrick, C. Gelatt, M. Vecchi, Science **220**(4598), 671–679 (1983)
S. Matej, A. Vardi, G. Herman, E. Vardi, in Discrete Tomography: Foundation, Algorithms and Application, ed. by G.T. Herman, A. Kuba (Birkhäuser, Boston, 1999), pp. 191–211
G. McKinnon, R. Bates, IEEE Trans. Biomed. Eng. **28**, 123–127 (1981)
N. Metropolis, A.W. Rosenbluth, M.N. Rosenbluth, A. Teller, E. Teller, J. Chem. Phys. **21**, 1087–1092 (1953)
J. Sanderson, IEEE Trans. Nucl. Sci. **26**, 2685–2688 (1979)
K. Sauer, C. Bouman, IEEE Trans. Signal Process. **41**, 534–548 (1993)
M. Vénere, C. Moreno, A. Clausse, R. Barbuzza, M. del Fresno, Nukleonica **46**(1), 5–6 (2001)
G. Winkler, Image Analysis, Random Fields and Markov Chain Monte Carlo Methods, A Matematical Introduction, 2nd edn. (Springer, Berlin, 2003)